Optics Letters

Time-resolved inline digital holography for the study of noncollinear degenerate phase modulation

N. V. Petrov,[1,*] S. S. Nalegaev,[1] A. V. Belashov,[1,2] I. A. Shevkunov,[1] S. E. Putilin,[1] Y. C. Lin,[3] and C. J. Cheng[3]

[1]ITMO University, 49 Kronverkskiy pr., St. Petersburg 197101, Russia
[2]Ioffe Institute, 26 Polytekhnicheskaya, St. Petersburg 194021, Russia
[3]National Taiwan Normal University, 88, Sec. 4, Ting-Chou Rd., Taipei 11677, Taiwan
*Corresponding author: n.petrov@niuitmo.ru

Received 13 April 2018; revised 2 June 2018; accepted 8 June 2018; posted 11 June 2018 (Doc. ID 328337); published 16 July 2018

Recent works demonstrated that digital time-resolved holography is the prospective approach to study nonlinear light–matter interaction processes. In this Letter, we present a straightforward inline holographic approach for studying degenerate phase modulation induced by an inclined collimated pump beam in the isotropic sample. The method is based on a minimization of the difference between experimentally acquired data and simulated inline holograms obtained from a numerical model of pump–probe interaction in optical nonlinear media. A sophisticated experimental data processing algorithm is implemented to provide high sensitivity and a signal-to-noise ratio eligible for soft interaction with a collimated pump beam. The integral phase shift determined by our method can be used to estimate the nonlinear refractive index and the relaxation time for material with a low damage threshold. We validated our approach for the case of soda-lime and BK7 glasses.

OCIS codes: (090.1995) Digital holography; (120.5060) Phase modulation; (190.3270) Kerr effect; (190.7110) Ultrafast nonlinear optics.

https://doi.org/10.1364/OL.43.003481

The investigation of optical nonlinear properties of materials attracts the attention of researchers and is motivated by the development of photonic and optoelectronic devices. Single- [1] and multi-beam [2–5] methods based on the excitation of the medium and the response observation in accordance with the existing theoretical model are used for the measurements of material optical nonlinear properties [6]. Recently, the pump-probe digital holography has been introduced as an approach to estimate a nonlinear refractive index by means of iterative matching of the results of numerical simulation and experiment [7] and the following advantages of the technique over previous methods were highlighted. Due to the high temporal and spatial resolution inherent in this technique, the signal is predominantly local. It provides the opportunity to recognize various physical processes in space and time. The soft spot of the technique is a complex light propagation model used to solve the nonlinear Schrödinger equation.

In this Letter, we contribute to the development of a given approach by presenting the algorithm of the probe beam integral phase shift calculation at the exit of nonlinear media. Our holographic arrangement of the probe beam is based on Gabor scheme. In contrast to the methods utilizing the focusing of radiation into the sample under study, in order to achieve a higher power density and induce stronger nonlinear response (e.g., [1,3,7]), we consider a lensless configuration where the pump beam is collimated [8]. It provides improved stability [9] and excludes experimental errors from the extra optics. It also decreases the power density of the pump beam at the sample which provides the opportunity to neglect self-focusing and, thus, to simplify the computational model, as well as to make this technique suitable for materials with a low damage threshold or inherent high absorption.

The registration of weak signals invokes the use of advantages of digital holography, among which an embedded signal processing and great potential for automatization and recording of statistically reliable data are crucial for a considered task. In this Letter, we consider isotropic homogeneous material, which allows us to calculate spatially averaged diffraction profiles carrying the information about nonlinear interaction. We will show that such image processing increases the signal-to-noise ratio (SNR) more than four orders of magnitude, provides a comparable sensitivity with other state-of-the-art methods [4] and, simultaneously, is able to replace more complex specialized equipment (e.g., necessary for lock-in amplification).

The experimental setup for the developed time-resolved inline digital holographic (TRIDH) approach is shown in Fig. 1(a). It is based on a Ti:sapphire laser system (regenerative amplifier Regulus 35F1K, Avesta Project, 2.3 mJ pulse, 35 fs pulse duration, 800 nm central wavelength, 30 nm spectral width, 1 kHz repetition rate). A laser beam with p-polarization is split on pump and probe beams, 96% and 2% of total energy, correspondingly. These beams cross in the horizontal plane

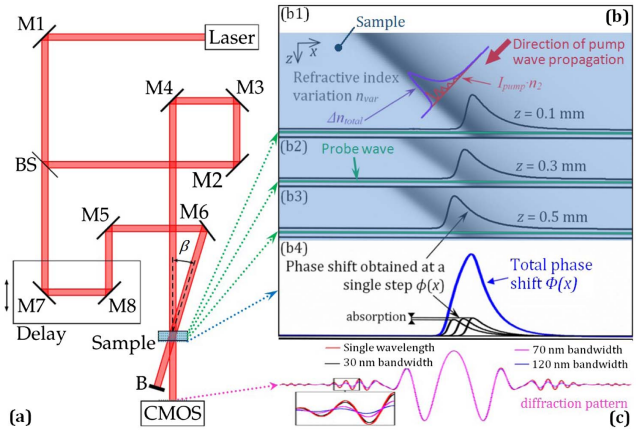

Fig. 1. (a) TRIDH setup and phenomena observed (b) inside the sample and (c) at the registration plane: a scheme of NDPM interaction (b1)–(b3) and $\Phi(x)$ formation at the exit of the sample (b4); FDPs formed at the registration plane for various spectral bandwidths of probe laser pulse (c).

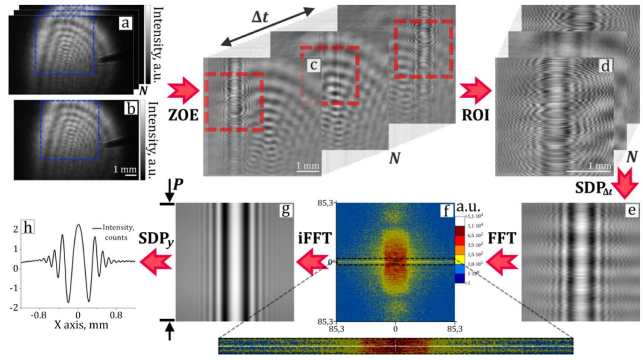

Fig. 2. Data processing: (a) N holograms recorded with varying Δt, (b) mean BG, (c) the results of the application of ZOE, (d) ROI, (e) SDP$_{\Delta t}$, (g) SF, (h) SDP$_y$; SF eliminates all except (mainly) narrow lines highlighted on the inset (f).

under adjustable acute angle β and overlap inside the investigated sample. The collimated pump beam with driven delay produces a variation of refractive index inside the homogeneous sample, which locally distorts the probe wavefront profile equally in the vertical direction. By analogy with Ref. [7], we introduce the term noncollinear degenerate phase modulation (NDPM) [10] in order to briefly define the phenomenon taking place. Because of the small spatial interaction region caused by the walk-off effect [11], the pump beam alters the phase change profile in a local region of the sample. Due to the fast relaxation of nonlinear refractive index variation of the sample, the phase shift of the probe beam is accumulated only inside the local area, outlined by the position of the beam profiles overlapping inside the sample. Figure 1(b) explains the NDPM process. The probe beam which carries the information about material response on NDPM diffracts during the propagation, and the result pattern is registered on the CMOS camera (1900 × 1200, 5.86 μm) in the form of averaged over $M = 15$ exposure inline holograms. Consistently delaying the pump beam on time Δt by the moving of a motorized linear translation stage, we shift the intersection volume along the x-axis and, thus, scan the sample. Then the registered series of images was subjected to comprehensive image processing to extract the useful signal and to obtain statistically reliable data.

Signal processing includes the following steps: zero-order elimination (ZOE) and spatial filtering (SF) conjugated with statistical data processing (SDP). The registered diffraction pattern is formed as a result of interference between the instant nonlinear signal of NDPM with an unperturbed background (BG). Due to the weakness of the nonlinear electronic photorefraction effect, the induced NDPM diffraction signal is much smaller compared to the BG intensity of the probe beam on the registered holograms. This leads to the dominance of BG energy with respect to the NDPM signal up to several tens of times; thus, there are no visible differences between the images (a) and (b) of Fig. 2. Similar to the work in Ref. [12], to extract Fresnel diffraction patterns (FDPs) [8] in the form of straight interference fringes along the vertical direction [see Fig. 2(c)], the ZOE technique was used. Here a zero-order term is considered as an averaged BG image, measured in the absence of a pump beam. Practically, it is calculated as averaging over all images recorded during the variation of time delay Δt. This ZOE algorithm implementation enhances an SNR by the factor $k_{ZOE} = \mathrm{SNR}_{ZOE}/\mathrm{SNR}_{raw} = \mathrm{STD}_{raw}/\mathrm{STD}_{ZOE}$, where STD is the standard deviation from simulated data, subscripts raw and ZOE denote the mean values for holograms before and after ZOE. For the FDP in Fig. 4(f) with the lower pulse energy, $k_{ZOE} \approx 55$ was estimated. To perform further image processing, a NDPM diffraction signal must be strongly perpendicular to the x-axis. To comply with this condition, a preliminary image rotation with an interpolation for a subpixel accuracy was used when necessary. SF is implemented to cut off a useful diffraction signal from parasitic oscillations. The algorithm [Figs. 2(e)–2(g)] consists of direct Fast Fourier transforms (FFTs) and 2D inverse FFTs with a narrow horizontal mask, shown in the inset of Fig. 2(f). SDP is the additional step used to obtain reliable data in the case of samples made from a homogeneous material. It includes the averaging of regions of interest (ROIs) [SDP$_{\Delta t}$, Figs. 2(d) and 2(e)] and averaging over the $P = 450$ image rows [SDP$_y$, Figs. 2(g) and 2(h)], as was performed in Ref. [13]. ROIs are extracted with subpixel accuracy over the series of processed images corresponding to the holograms captured with different Δt between the pump and probe pulses. For the case of the angle $\beta = 15°$, this Δt variation was realized by N steps of the linear stage (with step size $\Delta s = 2.5$ μm). Thus, the series of $N = 36$ holograms was recorded. SDP$_{\Delta t}$ is used to convert the data to a one-dimensional profile. In fact, this SDP$_{\Delta t}$ is the analog of a coherent noise reduction technique [14] if we assume that, instead of sample displacements, the area of NDPM is shifted by the scanning delay line. Thus, in the case of a homogeneous sample, due to the application of the SDP procedure, the spatial distribution of both beams does not affect the obtained result.

The images presented in Fig. 2 are targeted to show a typical case of the holograms obtained in our experiments (sample thickness $l = 1.08$ mm, pulse energy $E = 0.23$ mJ). The beams were distorted by parasitic diffraction, as is clear from Figs. 2(a) and 2(b). Figure 2(d) demonstrates selected ROIs with NDPM signals distorted by multiple concentric fringes appeared in a result of diffraction at sample surface inhomogeneities. Nevertheless, the eventually extracted signal from N holograms is clear from the artifacts imposed by poor

experimental conditions. The SNR enhancement due to the comprehensive digital image processing (Fig. 2) was estimated as $k_{\text{total}} = k_{\text{ZOE}} \cdot \sqrt{M \cdot N \cdot P} = 2.7 \cdot 10^4$ times in the assumption that noise is Gaussian. More solicitous experimental conditions with an increase in the number of averaged data can provide an additional increase in the SNR of at least 10-fold.

The pump-probe digital holography approach in Ref. [7] is based on the matching of the results of numerical simulations and experiments. Here we propose that a more simple simulation model suitable for our experimental configuration allows us to calculate of FDPs [8]. Consider the propagation and interaction of equally polarized pump and probe waves in optical media with linear n and nonlinear n_2 refractive indexes, correspondingly, wherein the probe wave is normally incident on the sample and propagates along z-axis. The pump wave is incident on the sample at an angle β and propagates at an angle $\theta = \arcsin(\frac{\sin\beta}{n})$ inside the sample in accordance with Snell's law. We assume that probe wave intensity is negligibly small to give rise to the refractive index variation, and the intensity of the pump wave I_{p} is high enough to induce nonlinear optical effects in the media. The profile of the pump wave in the temporal domain $I_{\text{p}}(t)$ can be approximately described as hyperbolic secant [15]. In this case, pump wave propagation in the nonlinear media leads to the generation of a nonlinear refractive index gradient, which exponentially decreases with relaxation time τ [Figs. 1(b1)–1(b3)]. Therefore, the probe wave with central wavelength λ acquires the total phase shift Φ [Fig. 1(b4)], which leads to its diffraction in a recording plane at a distance d [Fig. 1(c)]. In the general case, the absorption coefficient a of the pump wave should be taken into account.

A stepwise algorithm (six operations per step) based on a 2D model of NDPM was proposed to simulate FDPs:

(1) Nonlinear refractive index relaxation due to pump femtosecond pulse propagation in nonlinear media [see the difference in the red peaks in Fig. 1(b1)]:

$$n^i_{\text{var}}(x,z) = n^{i-1}_{\text{var}}(x,z)\exp^{-\Delta t/\tau}. \quad (1)$$

(2) Spatial shift of the pump pulse in nonlinear media:

$$\tilde{I}^i_{\text{p}}(z,x) = I^{i-1}_{\text{p}}\left(z + \frac{c}{n}\Delta t\ \cos(\theta), x + \frac{c}{n}\Delta t\ \sin(\theta)\right). \quad (2)$$

This leads to the difference in the x-position of the refractive index gradient in Figs. 1(b1)–1(b3).

(3) Decrease in pump pulse intensity due to absorption:

$$I^i_{\text{p}} = \tilde{I}^i_{\text{p}}\exp^{-a/(\frac{c}{n}\Delta t)}. \quad (3)$$

This leads to the difference in black peaks of $\phi(x)$ in Fig. 1(b4).

(4) Increase in refractive index variation due to nonlinearity:

$$n^i_{\text{var}}(x,z) = n^{i-1}_{\text{var}}(x,z) + I^i_{\text{p}}(x,z)n_2. \quad (4)$$

(5) Shift of the probe pulse along the z-axis:

$$z^i_{\text{pr}} = z^{i-1}_{\text{pr}} + \frac{c}{n}\Delta t. \quad (5)$$

(6) Increase in phase shift of probe beam:

$$\Phi^i(x) = \Phi^{i-1}(x) + \frac{2\pi\frac{c}{n}\Delta t n_{\text{var}}(x,z)\delta(x - x_{\text{pr}}, z - z_{\text{pr}})}{\lambda}, \quad (6)$$

where the delta function is used to calculate the location of the probe beam. The algorithm is performed until the probe wave reaches the exit plane of the object at thickness $z = l$.

Thus, at the end of the stepwise algorithm, the integral phase shift distribution $\Phi(x)$ at the exit of the sample will be obtained. Further calculation of the FDP was performed by means of numerical propagation of the probe wavefront to the registration plane using an angular spectrum algorithm [16]. Note that in contrast with the experimental study neither noise nor BG, eliminated in the data processing procedure, were added to the diffraction pattern in numerical simulation.

The described approach implies the simulation of FDPs for a monochromatic probe wave [Fig. 1(c)]. In the case of ultrashort probe pulse in order to take into account its broadband nature, a calculation of FDPs for all the wavelengths of the laser pulse bandwidth and summation of obtained intensity distributions should be performed. This leads to a decrease of the intensity pattern modulation amplitude for side maxima. However, for a 30 nm bandwidth of the laser system utilized in our case, the effect is negligible (STD = 0.005%; Fig. 1(c)).

The diffraction pattern in the registration plane depends on a number of experimental parameters: propagation distance d, sample thickness l, angle of incidence β, absorption coefficient a (measured directly), and nonlinear refractive index n_2 and its relaxation time τ. Dependencies between the given input parameters and the observed diffraction pattern can be revealed from numerical experiments. Four sets of integral phase shift distributions and diffraction patterns corresponding to the distance $d = 120$ mm are presented in Fig. 3. By default, the simulation parameters were set as $l = 1$ mm, $\tau = 50$ fs, $\beta = 31.2°$, $a = 0.01$ cm^{-1}, and $n = 1.515$. In each column, a single parameter was varied in order to observe its impact on the resultant diffraction pattern. It was found that a change of l results in a proportional change of induced phase shift and diffraction pattern contrast. The shape of the phase shift distribution, as well as the location and number of side maxima on the diffraction pattern depends on θ. The variation of α leads to minor change in the shape of phase distribution and the side maxima location. Increase of τ leads to a rise of asymmetry in phase and intensity distributions. Such asymmetry can be observed in one of our experiments [see Figs. 4(a) and 4(b)].

A comparison between experimental and simulated FDPs obtained from the numerical model of NDPM was performed for two experimental conditions. First, inline digital holograms were recorded on a CMOS sensor at $d = 55$ mm, incident angle $\beta = 28°$, and sample thicknesses of 0.94 and 0.69 mm, processed and juxtaposed with simulated ones [Figs. 4(a) and 4(b)]. Normalized STD σ_{norm} between the experimental and simulated FDPs was used for fitting optimization and estimation of free parameters $\Delta\Phi_{\text{max}}$ and τ. Three samples were studied: (1) soda-lime glass $l_1 = 1.08$ mm (2) BK7 glass

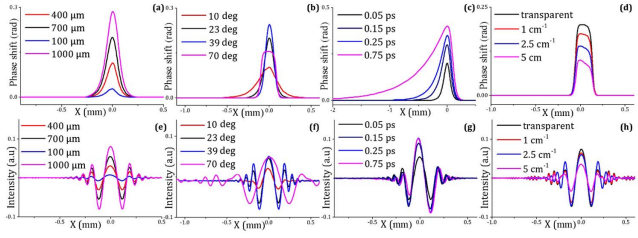

Fig. 3. (a)–(d) Integral phase shifts and (e)–(h) NDPM diffraction patterns for various (a), (e) sample thicknesses l; (b), (f) angle β; (c), (g) relaxation times τ; and (d), (h) absorption coefficients.

$l_2 = 0.94$ mm, and (3) BK7 glass $l_3 = 0.16$ mm in slightly different experimental conditions $\beta = 15°$ and $d = 101.5$ mm. Inline holograms were captured for each sample at various pump pulse energies. Typical dependence $\sigma_{\text{norm}}(\Delta\Phi_{\max}, \tau)$ corresponding to the FDP at $E = 2.08$ mJ in Fig. 4(d) is shown in Fig. 4(c). The estimated σ_{norm} and $\Delta\Phi_{\max}$ values, as well as the corresponding experimental and simulated FDPs, are shown in Figs. 4(d)–4(f). For the case of the weakest FDP signal shown in Fig. 4(f), $\Delta\Phi_{\max} \approx \lambda/1430$. By reducing the pulse energy to $E \approx 24$ μJ as in Ref. [4], we could determine the order of our minimum detectable time averaged $\langle \Delta n_{\text{total}} \rangle$ as 10^{-8} which corresponds to a minimal induced $\Delta\Phi_{\max} \approx \lambda/13700$. The sensitivity can be increased by the optimization of angle β, sample thickness l, the camera's FOV, intensity I, step size Δs (due to $\text{SDP}_{\Delta t}$), and by minor amendings of the ROI or $\text{SDP}_{\Delta t}$ algorithms.

The obtained results show that σ_{norm} between experimental and simulated FDPs is about 1%–3%. Although some disagreements between experimental and numerical data are clearly seen in Fig. 4(f), they mostly occur in high-order diffraction maxima. The mismatch can be explained by experimental errors; one of them is especially obvious in Fig. 4(d). Taking into account linear proportionality between the induced phase shift and both sample thickness and pump pulse energy, $\Delta\Phi_{\max}$ determination accuracy is estimated as 10–15%.

The expected value of the calculated refractive index relaxation time for all the studied samples in the second set of experiments is 16 fs with STD = 28.5 fs, which is in good agreement with previous estimations reported in Ref. [17]. An approximate estimation with an order of magnitude accuracy of the pump beam intensity at the sample input $I_{\text{pump}} \approx 7 \cdot 10^9$ W/cm^2 for $E = 0.23$ mJ allowed us to estimate n_2 for soda-lime and BK7 glass as $1.25 \cdot 10^{-15}$ cm^2/W and $9 \cdot 10^{-16}$ cm^2/W, correspondingly, with accuracy of the order of magnitude. The obtained values are in an agreement with known data [18].

In conclusion, we have presented Time-Resolved Inline Digital Holography approach for investigation of pump pulse-induced phase variation in transparent samples with Kerr-type optical nonlinearity. We fully described and explored the process of inline time-resolved hologram formation, and developed a stepwise algorithm for the simulation of NDPM.

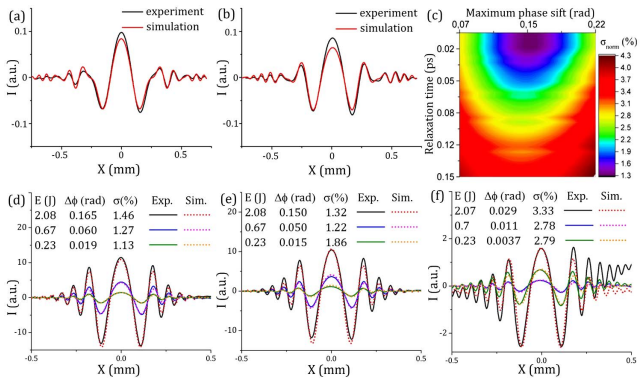

Fig. 4. Experimentally and numerically obtained diffraction patterns corresponding to glasses with thicknesses of (a) 0.94 and (b) 0.69 mm. (c) Typical dependence $\sigma_{\text{norm}}(\Delta\Phi_{\max}, \tau)$ for glasses with thicknesses (d) l_1, (e) l_2, and (f) l_3.

A comparison of the simulation and the experiment allows us to estimate the integral phase shift at the exit sample plane as well as the sign, magnitude, and relaxation time of the nonlinear refractive index by the calculation of NDPM dynamics.

In this Letter, we implemented image processing techniques to increase signal sensitivity in the experimental observations. Based on the procedures of the automated processing of a large series of images for isotropic material, we extracted accurate data about the weak modulation of the diffraction pattern on the inline holograms. Due to digital holography principles, this allows us to significantly simplify the experimental scheme and, at the same time, provides comparable sensitivity of Δn estimation compared with a beam deflection approach [4].

Currently, in the task of studying homogeneous samples, we utilize spatial signal diversity to increase an SNR. The developed approach is most attractive for materials with a low damage threshold and inherent high absorption. A further expansion of the technique for spatially inhomogeneous samples is able to provide the characterization of their local nonlinear properties. We believe that the local measurements of nonlinear properties promise a great progress in the material sciences and related areas. In particular, the developed technique has potential for fast investigation of the set of the nonlinear micro-objects possessing spatial diversity in their nonlinear properties, e.g., arrays of quantum dots.

Funding. Ministry of Education and Science of the Russian Federation (Minobrnauka) (3.1893.2017/4.6, 3.9041.2017/7.8); Russian Foundation for Basic Research (RFBR) (16-52-52049\16); Ministry of Science and Technology, Taiwan (MOST) (105-2923-E-003-001).

REFERENCES

1. M. Sheik-Bahae, A. Said, T.-H. Wei, D. Hagan, and E. Van Stryland, IEEE J. Quantum Electron. **26**, 760 (1990).
2. S. Friberg and P. Smith, IEEE J. Quantum Electron. **23**, 2089 (1987).
3. M. Sheik-Bahae, J. Wang, R. DeSalvo, D. J. Hagan, and E. W. Van Stryland, Opt. Lett. **17**, 258 (1992).
4. M. R. Ferdinandus, H. Hu, M. Reichert, D. J. Hagan, and E. W. Van Stryland, Opt. Lett. **38**, 3518 (2013).
5. S. S. Nalegaev, A. V. Belashov, and N. V. Petrov, Opt. Mater. **69**, 437 (2017).
6. C. B. de Araújo, A. S. L. Gomes, and G. Boudebs, Rep. Prog. Phys. **79**, 036401 (2016).
7. B. Momgaudis, S. Guizard, A. Bilde, and A. Melninkaitis, Opt. Lett. **43**, 304 (2018).
8. M. G. Beygi, R. Karimzadeh, and M. Dashtdar, Opt. Laser Technol. **66**, 151 (2015).
9. M. Terazima, Opt. Lett. **20**, 25 (1995).
10. Q. Z. Wang, P. P. Ho, and R. R. Alfano, Opt. Lett. **15**, 1023 (1990).
11. N. V. Petrov, S. E. Putilin, and A. A. Chipegin, Appl. Phys. Lett. **110**, 161107 (2017).
12. M. Lihong, W. Hui, L. Yong, and J. Hongzhen, Opt. Express **20**, 1805 (2012).
13. A. Belashov, Y. Beltukov, N. Petrov, A. Samsonov, and I. Semenova, Appl. Phys. Lett. **112**, 121903 (2018).
14. F. Pan, W. Xiao, S. Liu, F. Wang, L. Rong, and R. Li, Opt. Express **19**, 3862 (2011).
15. M. E. Fermann, A. Galvanauskas, and G. Sucha, *Ultrafast Lasers—Technology and Applications* (CRC Press, 2003).
16. J. W. Goodman, *Introduction to Fourier Optics*, 3rd ed. (2004).
17. M. Yamane and Y. Asahara, *Glasses for Photonics* (Cambridge University, 2000).
18. K. Jamshidi-Ghaleh, N. Mansour, and A. Namdar, Laser Phys. **15**, 1714 (2005).